

Transport Mechanisms in Smectite Clay Control Migration of Radionuclides Escaped from Disposed Nuclear Waste

Roland Pusch¹

Abstract

At present two ideologies appear to govern the international selection of concepts for isolation of radionuclides escaped from High-Level Radioactive Waste (HLW) stored underground: “shallow” burial in mined repositories in crystalline rock, and deep geologic disposal in holes bored in crystalline or sedimentary rock, making use of metal canisters isolated from the rock by concrete or dense expansive clay. The present paper describes disposal in smectite clay for delaying or preventing radionuclides from reaching the biosphere when they can still cause great havoc. This is achieved by utilizing the great waste-isolating capacity of the expansive clay through its high hydrophilic capacity and large specific surface area, providing low porosity and limited interconnectivity of the voids, which both makes such clay low-permeable and operating with a very low through-diffusion rate of anionic species like iodine, and of some cationic radionuclides. The expandability of such clay means that it can swell and undergo self-healing in case of microstructural contraction caused by heating. The mechanisms involved in permeation and ion exchange are described based on conceptual microstructural models and their theoretical analogies. Stress/strain phenomena involved in saturation with fluids, desiccation, shearing under deviatoric conditions, and creep strain under stable conditions or at failure are described as well. Longevity matters are given limited space.

Keywords: Nuclear Waste, High-Level Radioactive Waste (HLW), smectite clay, migration of radionuclides.

¹ Lulea Technical University, Lulea, Sweden.

1. Scope of Study

Disposal of radioactive waste is suitably made underground in stable crystalline rock at several hundred or thousand meters depth, utilizing the host rock for mechanical protection, and engineered barriers of clay for limiting migration of radionuclides to the surroundings of the repository. In this document we consider the performance of smectite clay with respect to migration of radionuclides possibly emanating from stored highly radioactive waste, like spent nuclear fuel disposed in bored holes.

2. Smectite Clay Crystal structure

The basic units consist of stacked lamellae each of them consisting of two sheets of SiO_4 tetrahedrons confining a central octahedral layer of hydroxyls and Fe, Mg or Li ions (Figure 1). In this document we will deal with clays dominated by montmorillonite which has only Si in the tetrahedrons and Al in the octahedrons, focus being on transport of porewater and solutes. In this document we prefer to refer to the crystal constitution of Edelman/Favejee's (EF) model since it can explain the negative charge of montmorillonite crystal lattices and serve as a basis for exploring hydration phenomena related to this smectite species.

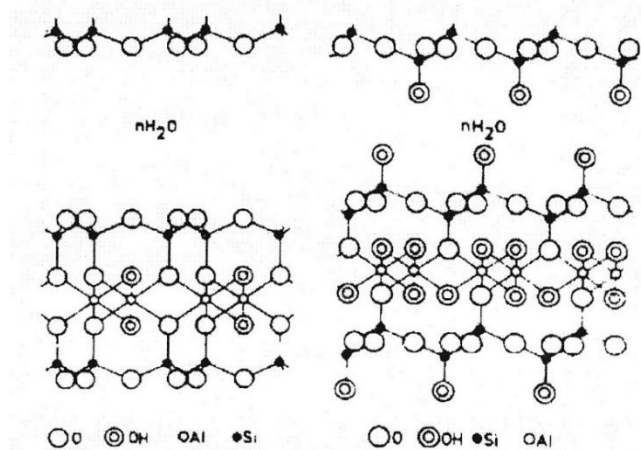


Figure 1: Two possible lattice constitutions of montmorillonite.
Left: Hofmann, Endell and Wilms' "high-temperature" (>100°C) version.
Right: Edelman and Favejee's "low-temperature" (<60°C form), (Forslind and Jacobsson, 1975). The interlamellar space can host water molecules, cations and charged molecules. The unhydrated lamellae have a thickness of 1nm.

3. Interlamellar Hydration of Smectites

Forslind and Jacobsson introduced a structural model for interlamellar water based on Edelman/Favejee's crystal lattice constitution of montmorillonite (Forslind and Jacobsson, 1972). It partly explains the discrepancy in cation exchange capacity, i.e. that the EF model gives a six times higher CEC value than experiments, but agrees with them if the apices carrying acidic hydroxyls are assumed to exchange their protons. According to these investigators the first associated water lattices are coupled to the basal planes of the crystallites assuming that the water is ice-like. Figure 2 shows the protruding hydroxyls of the (001) plane with three unit cells, and exhibiting also the basal molecules of a superimposed ice lattice. One finds that there are only four hydrogen bonds formed between the three unit cells and the water lattice and that the charge should therefore attain a mean value of two-thirds of a charge unit per crystal cell. This is also the average CEC-value recorded.

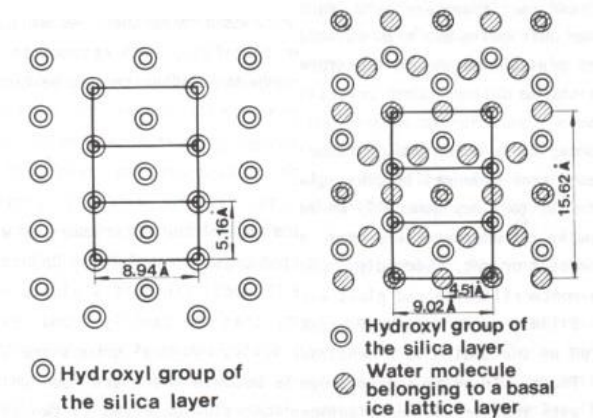


Figure 2: Left: Protruding hydroxyls of the (001) plane with three unit cells shown. Right: The basal molecules of an ice lattice superimposed on these hydroxyls (Forslind and Jacobsson, 1972).

A consequence of this is that the water molecules are not as closely packed as in bulk water and that the water density is hence lower than 1000kg/m^3 , excepting the cations present. A special feature of the Forslind/Jacobsson crystal/water model is that expulsion of protons from the lattice apices causes a negative particle charge. This can explain the negative charge of montmorillonite particles without assuming isomorphous substitutions and vacancies in the crystal lattices.

The small Na and Mg cations in interlamellar positions do not disturb the water lattice, while disturbance is caused by large cations and by those having strong affinity to water like Ca (Sposito, 1984). By exchange of Na for Ca the solvation shell of the latter ion binds water so effectively that the water lattice is disturbed and is no longer strongly associated with the lattice oxygens as implied by the Forslind/Jacobsson's model. The water molecules in the interlamellar space are organized such that the first hydrate is thicker than the second and that no more

hydrates can be formed. The change in organization of water molecules in Forslind's and Jacobsson's model on replacing Na-montmorillonite by Ca in the interlamellar space can involve conversion of the structural constitution from Edlmann/Favejee's form to that of Hoffman/Endell/Wilm's model. This would imply a change in coordination of tetrahedral Si and octahedral Al, which should be detectable by using spin-spin NMR technique as has in fact been done (Pusch, 1993).

For the Na-state the hydrate layers according to the Forslind/Jacobsson model have been proposed to be as indicated in Figure 3, implying that only certain water lattice configurations are stable. The stable monolayer yields a d -spacing of 17.81 Å and a water content $w=11.9\%$. For two layers $d=22.4$ Å and $w=23.8\%$ and for three layers $d=25.17$ Å and $w=35.7\%$. These values fit with published (002) and (003) data (Kehres, 1983), hence making the hydration model trustworthy. However, careful analysis of recent XRD data show that hydration of smectite-rich samples do not give perfectly regular water layer sequences and the geometry and density variations of hydrated smectites are still not accurately known.

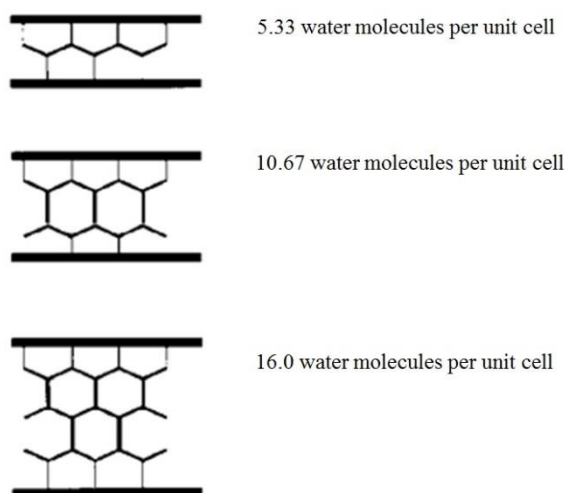


Figure 3: Model of hydrate configuration in the interlamellar space of montmorillonite with Forslind's/Jacobsson's crystal constitution. The stable monolayer yields a d -spacing of 17.81 Å and a water content $w=11.9\%$, while it is $d=22.41$ Å for two layers and $d=25.17$ Å for three layers.

The organization of clay particles, coarser grains and organic matter, which together make up the solid phase, and the degree of water saturation, determine the physical properties of clays. The interlamellar, often called “internal” water, dominates over the free or “external” water at high dry densities especially in Na-montmorillonite (Figure 4).

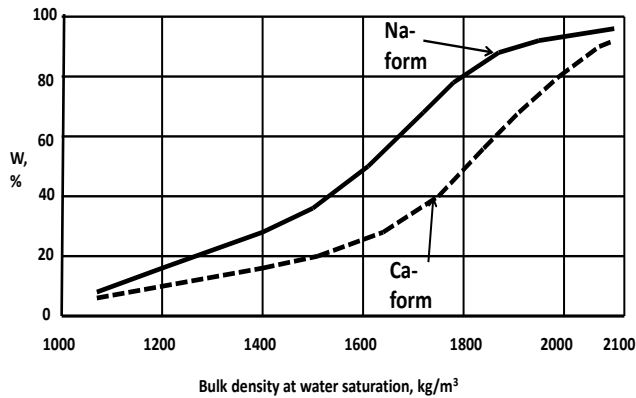


Figure 4: Fraction of interlamellar water in montmorillonite (Pusch and Yong, 2006, Pusch et al, 2012). At complete water saturation the interlamellar water constitutes at least 80% of the porewater in Na clay with 1270kg/m³ dry density. For Ca in exchange position the corresponding percentage is about 50.

Figure 5 summarizes schematically how the crystal constituents join to form smectite lamellae. Forces keeping the lamellae together are weak allowing for easy separation of them.

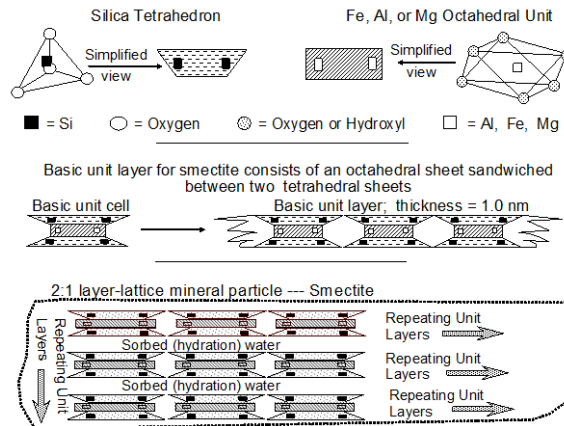


Figure 5: Stacking of unit layers with the interlamellar space occupied with hydration water (After Yong). This space is often termed “internal” for distinguishing it from the “external” space between particles, i.e. stacks of lamellae (After Yong).

Hydration of the interlamellar space depends on the charge and coordination of adsorbed cations and water molecules (Pusch, 1987, 2015). A water hull, one monolayer thick and containing cations, is sorbed on the basal surfaces of practically all minerals, and plays a role in diffusive ion transport and in osmotic swelling of smectites. The interlamellar hydrates determine the swelling potential, while the hydrated surface properties of the stacks of lamellae determine the bulk plasticity and rheological behaviour. The coordination of interlamellar water molecules and cations and the crystal lattice atoms depends on the size and charge of the cations and of the charge distribution in the lattice. Three hydrate layers can only be formed in the smectite species montmorillonite, and normally only when sodium, lithium or magnesium are in interlamellar positions. When Na is in the interlamellar space the coupling to water molecules is weak and the cations relatively free to move, which indicates that the interlamellar water molecules form their own H⁺-bonded structure (Fig.3), while in Ca-smectite the cations are strongly hydrated and the interlamellar complexes are rigid and stable. This means that the swelling pressure and the pressure required to expell interlamellar water is higher for Ca-smectite than for Na-smectite for dry bulk densities exceeding about 1600 kg/m³. The much higher mobility of Na ions taken up from a NaCl solution is in agreement with the significantly higher diffusion coefficient (Figure 6).

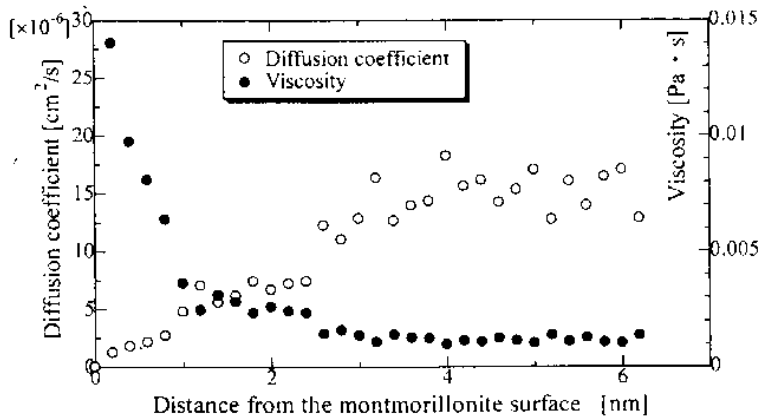


Figure 6: Diffusion coefficient and viscosity of montmorillonite clay calculated by use of molecular dynamics (After Ichikawa).

From a practical point of view, the different physical constitutions of interlamellar water is believed to be that the stacks of lamellae in Ca-montmorillonite, i.e. the clay “particles”, are much stronger and less easily disrupted than in Na-montmorillonite giving the first-mentioned a character of silty, frictional-type soil with less potential to form gels. Ca-montmorillonite is hence believed to be stiffer and undergo less creep strain than Na-montmorillonite exposed to the same deviator stress. In both types the interlamellar water is believed to be more viscous than ordinary water and to be largely immobile under normal hydraulic gradients.

4. Extra-lamellar Hydration

External surfaces are basal planes and edges of the stacks of lamellae along which solutes, cations and molecules migrate driven by porewater flow, concentration gradients and electric potentials. The surfaces consist of hexagonal arrangements of oxygens or hydroxyls and can attach water molecules by establishing hydrogen bonds (Figure 3). Where basal planes come close electrical double-layers interact. They have relatively high concentrations of cations near the mineral surface, which affects the organization and physical state of the hydrates (Figure 7).

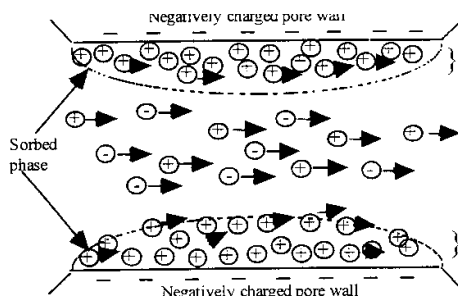


Figure 7: Interacting electrical double-layers. The intermediate space offers large amounts of hydration sites due to the crystal lattice constitution, which determines the charge and co-ordination of adsorbed cations and water molecules (After Neretnieks, 1993).

Figure 8 implies that the first few hydrate layers on smectite surfaces (Water A) are more viscous than those in Water B, which is, in turn, less viscous than the normally structured Water C. These issues are of fundamental importance for understanding transport processes in smectite clay.

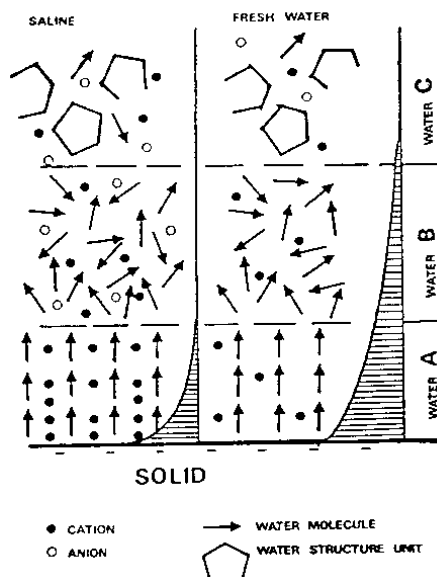


Figure 8: Proposed organization of water and ions at clay mineral surfaces. Water A is largely immobile by being coupled to surface atoms. Water B is low-viscous. Water C is free with normal viscosity. Hatched areas represent the charge distribution in the electrical double-layers (Left: Salt water, Right: Fresh-water). (After Drost-Hansen).

Table 1 shows the number of hydrate layers close to the basal planes of montmorillonite crystals representing Water A with Na or Li cations according to Colten, 1986.

Table 1: Number of hydrate layers in compacted Na montmorillonite with 1200kg/m³ dry density as a function of the water content (Colten, 1986). The clay was saturated with distilled water. Notice the fair agreement with data in Figure 4.

Water content, % (by weight)	Number of hydrates
<7	0
7-10	1
10-20	1-2
20-25	2
25-35	2-3
>35	3

5. Preferential Paths for Pore Water Flow

The organization of repeated microstructural units in Figure 5 indicates that there are preferential paths for migration of water and solutes along and within in aggregated smectitic clays. Such paths can be formed where stacks of lamellae interact, i.e. where electrical double-layers are established and where the most narrow space filters off anions and molecules (Figure 7).

A very common microstructural feature is series of coupled voids forming channels, a matter that has been thoroughly investigated by several investigators of which Bouchelaghem and Pusch (2017) have recently published data for tests in 2D (cf. Figure 9). They modeled hydraulic transmission using TEM electron images distinguishing between different microscopic scales using digitalized images and experimental conductivity data.

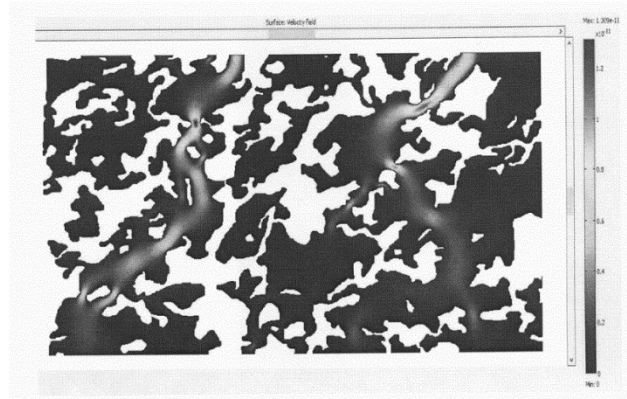


Figure 9: Steps in calculating hydraulic conductivity of 2D digitalized electron micrographs of montmorillonite (Bouchelaghem and Pusch, 2017). Identified connected macropores making up microstructural channels. Vertical scale represents the distribution of the hydraulic conductivity.

An early attempt by Pusch and Yong (2006) formed the basis of their study, an example of micrographs of impregnated and ultramicrotomy-cut smectitic clay appearing in Figure 10.

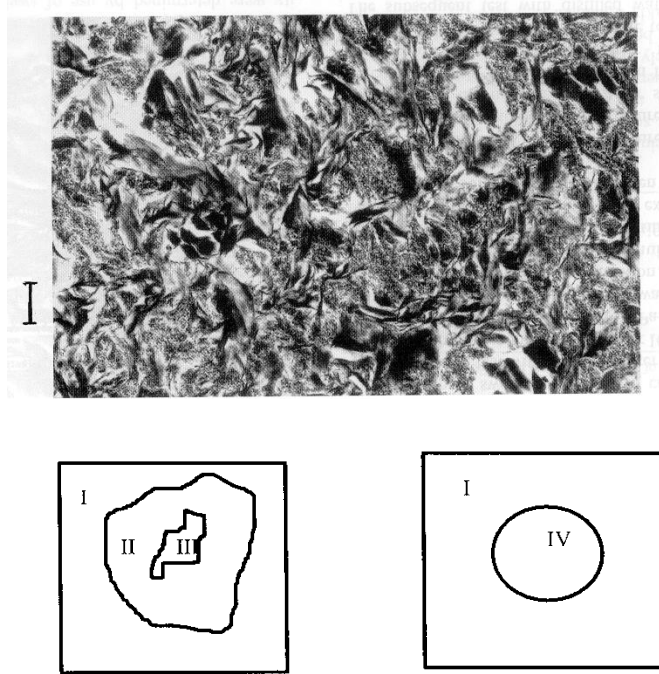


Figure 10: Upper: TEM micrograph of 500Å ultrathin section of clay with about 50% expandable minerals and 1900kg/m³ bulk density at water saturation (dry density 1430kg/m³). Darkest parts are minerals, while white parts are open voids. The bar is 1µm long. Lower left: Soft matrix (I to III). Lower right: Channel sections (Pusch, Muurinen et al, 1999).

The subsequent, more sophisticated study by Bouchelaghem and Pusch involved mathematical refinement and application of finite element analysis, giving good examples of channeling as exemplified by Figure 9. The dominant part of the clay matrix contains relatively few “macropores” that are supplied with percolating porewater by large numbers of very fine capillaries.

Numerical computations allowed the authors to investigate the contribution to macroscopic flow of the soft and dense gels in connected and non-connected configurations (cf. Figure 10). The study strongly supports the relevance of a third model shown in Figure 11 for through-flow of smectite-rich clay considered as a system of gel-filled channels of different size being similar to the model proposed by Neretnieks and Moreno (1993) and manifested by their 3Dchan code. It has been successfully used for modelling flow through soft, medium-dense and dense smectite clays (Pusch et al, 2001).

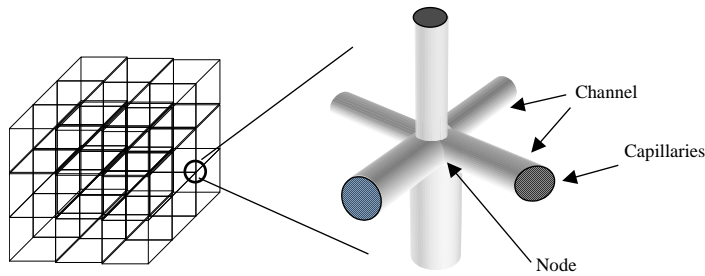


Figure 11: Channel network mapped as a cubic grid with channels intersecting at a node in the grid (Neretnieks & Moreno, 1993).

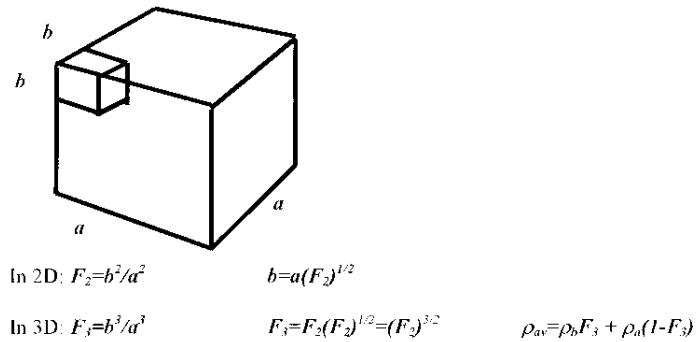


Figure 12: Definition of microstructural features in 2D and 3D assuming cubic symmetry.

Useful microstructural parameters introduced some decades ago are the size (maximum diameter) of discernible voids, and the P/T ratio with P representing the sectioned voids, i.e. IV in the right picture of Figure 10, and T = the total section area. The latter can be correlated to the bulk hydraulic conductivity of natural clays deposited in fresh or salt water. Statistical treatment can be made of suitably defined microstructural parameters, taking the solid clay matrix to consist of two major components (Pusch et al, 2006), i.e. (a) = stacks, stack aggregates and non-smectite grains, gel-filled voids, and (b) = unfilled voids This distinction was made on the ground that the first mentioned component is physically stable and largely impermeable while the latter offers little or no flow resistance. A further reason is that component a is largely responsible for the swelling pressure. Ion migration in this component primarily takes place by matrix and surface diffusion (Figure 13), while ion migration in b -space is almost entirely by pore diffusion.

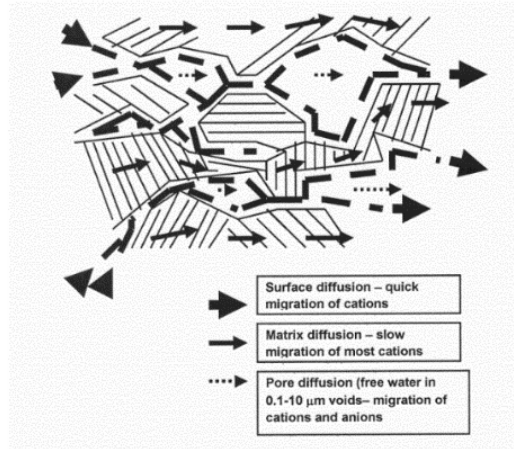


Figure 13: Smectitic clay with dense particle aggregates in the a-component shown as hatched areas.

The microstructural components are related through the coefficients F_2 for 2D and F_3 for 3D conditions, the ratio of which depends on the average and individual bulk densities as defined in Figure 12 and exemplified in Figure 14 for Wyoming bentonite. This procedure for density-related microstructural characterization can be applied to any soil analyzed with respect to the microstructural constitution using micrographs. of very thin sections.

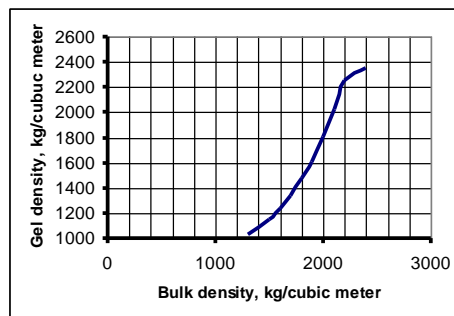


Figure 14: Relationship between microstructural parameters in 2D and 3D for Wyoming bentonite (MX-80). ρ_{av} is the average bulk density of the clay and ρ_a and ρ_b the average density of components a (stacks, stack aggregates and non-smectite minerals) and b (soft gel fillings and open space).

6. Quantification of Clay Microstructure

6.1 The F-parameters

Figure 12 defines the two microstructural parameters F_2 and F_3 for quantifying the hydraulic conductivity of clay elements in digitalized TEM micrographs based on their grayness which can be related to the density of the elements according to fundamental optical theory (Pusch and Yong, 2006). The variation in grayness can be converted into different colours for easy interpretation and representation of the variation of density (cf. Figure 15).

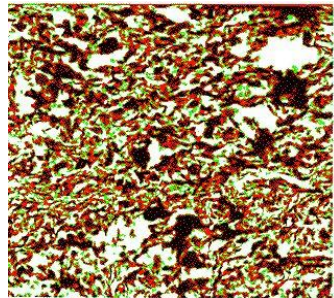


Figure 15: Example of digitalized micrograph of Wyoming bentonite (MX-80) with a bulk density at saturation of 1800kg/m^3 (dry density 1270kg/m^3). Black=densest parts of clay matrix *a*. Red=relatively dense parts of the same component. Green= soft, porous parts of component “*b*”. White represents open parts of this component, i.e. “*b*”. Edge length of micrograph is $3\mu\text{m}$.

Dominance of open voids and soft gels at high image magnification gives very high F_2 values and hence also F_3 -values, while interpretation of micrographs dominated by dense aggregates gives very low F_2 and F_3 . For smectite-rich clays micrographs with an edge length of at least $30\mu\text{m}$ are representative of the larger part of the clay matrix. F_2 and F_3 are related to the average bulk density of the clay as illustrated in Figures 16 and 17.

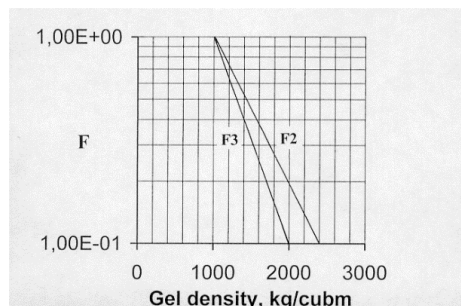


Figure 16: F_2 and F_3 versus gel density at water saturation for Wyoming bentonite (MX-80). Data based on microstructural analyses using $300\text{-}400\text{ \AA}$ ultramicrotome-cut sections.

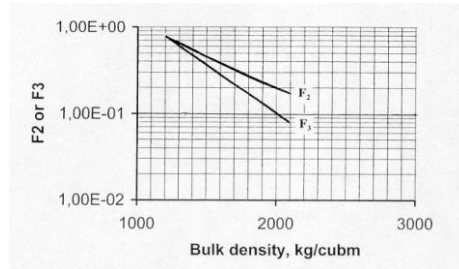


Figure 17: F_2 and F_3 versus bulk density at water saturation for Wyoming bentonite (MX-80).

From such diagrams, analytic expressions of parameters F_2 and F_3 can be derived as functions of the bulk density at saturation ρ_{bs} and the gel density at water saturation ρ_{gs} . We will show here how these microstructural parameters are related to the hydraulic conductivity, ion diffusivity, and to the swelling pressure.

6.2 Hydraulic conductivity

We will assume that the microstructure consists of systems of elements with different hydraulic conductivities giving the clay a representative average conductivity K determined by oedometer testing (cf. Pusch and Yong, 2006). Focusing here on the use of the F parameters for checking the relevance and usefulness of the procedure for quantifying microstructure by comparing experimentally obtained bulk hydraulic conductivity data for Na and Ca smectite clay, we will use the system of elements with different hydraulic conductivities in Figure 18.

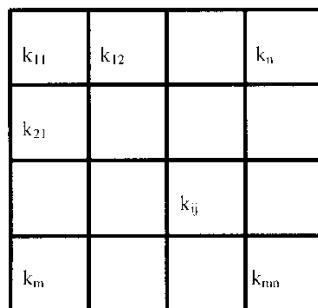


Figure 18: System of elements with different hydraulic conductivities, percolated horizontally.

The mean hydraulic conductivity K of clay with elements having different conductivities can be expressed as follows:

$$K=1/m [\sum_{(1 \text{ to } m)} n(\sum_{(1 \text{ to } n)/kij})^{-1}] \tag{1}$$

where:

- K = average hydraulic conductivity
- n = number of elements normal to flow direction
- m = number of elements in flow direction
- kij = hydraulic conductivity of respective element

The cross-sectional areas of individual voids identified in micrographs, together with the corresponding K -value calculated from Equation (1), have been compared with experimentally obtained data, and found to agree satisfactorily. Considering the uncertainty in estimating interconnectivity and tortuosity of the gel-filled voids and channels, and distinguishing only between permeable and impermeable fractions of the sections as a first order simplification, this approach appears to be reasonable. The fraction F_2 representing the permeable gel-filled fraction of REV sections² can thence be used for calculating K . The conductivity of the clay gels is assumed to be similar to the experimentally determined conductivity of clay with the same bulk density. F -data together with the calculated K -values are shown in Tables 2 and 3 for three representative bulk densities. Good agreement is obtained between the model-derived data for artificially prepared Wyoming clay (MX-80) and experimentally determined results and natural clay of the same type.

Table 2: Microstructural data and conductivities for MX-80 in Na form saturated and percolated by distilled water.

Bulk density [kg/m ³]	F_2	Gel density [kg/m ³]	Gel conductivity [m/s]	Calculated bulk conductivity [m/s]	Experimental bulk conductivity [m/s]	Porosity
2130 Na	0.17	2000	7E-14	E-14	2E-14	0.13
1850 Na	0.24	1650	2E-12	4E-13	3E-13	0.20
1570 Na	0.40	1150	2E-10	8E-11	8E-11	0.47

The microstructural heterogeneity of artificially prepared MX-80 clay is a significant factor for selection of a representative hydraulic conductivity of the clay in question for calculation purposes. In comparison with natural sedimentary clays with the same density and smectite content, the results indicate that higher

² REV=Representative elementary volume

hydraulic conductivity values are obtained for the artificially prepared MX-80 clay. The reason is that the natural clay has undergone long-term homogenization by creep and chemically induced changes in the time perspective of thousands of years, while the artificially prepared clay has not.

Impact of cation exchange is exemplified by considering the function of double-layer interaction (DDL): interaction of the stacks of lamellae by cation replacement of Na^+ by Ca^{2+} will raise the hydraulic conductivity. For the same F_2 values and gel densities as for MX-80 in Na form, data for MX-80 in Ca form appear in Table 3 for appropriate Ca gel conductivities.

Table 3: Microstructural data and conductivities for MX-80 in Ca form saturated and percolated by strongly brackish Ca-dominated water (Pusch and Yong, 2006).

Bulk density [kg/m ³]	F_2	Gel density [kg/m ³]	Gel conductivity [m/s]	Calculated bulk conductivity [m/s]	Experimental bulk conductivity [m/s]	Porosity
2130	0.17	2000	2E-13	3E-14	3E-14	0.13
1850	0.24	1650	8E-11	2E-12	2E-12	0.20
1570	0.40	1150	7E-5	3E-06	2E-09	0.47

The role of cation exchange on the hydraulic conductivity is demonstrated by Figure 19 for tests on MX-80 with 1800kg/m³ density saturated and percolated by 3.5% CaCl_2 solution. The initial rise in hydraulic conductivity was due to dislodgement of particles, which, together with the resultant non-homogeneous gel formation in the voids, became void pluggers as witnessed by the drop in the hydraulic conductivity after one day (Pusch and Yong, 2006).

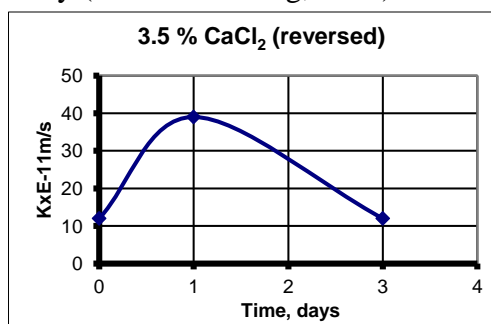


Figure 19: Change in hydraulic conductivity at 30m/m hydraulic gradient of smectite clay with 1800kg/m³ total density saturated with distilled water (1270kg/m³ dry density) followed by reversed flow with 3.5% CaCl_2 solution. Disruption of gels caused the initial rise while clogging led to the subsequent drop.

6.2 Ion diffusivity - Mechanisms involved

We will firstly consider a basic theoretical model of diffusion of adsorbed spherical Brownian particles in a porous medium (smectite clay), composed of zones of parallel planar surfaces representing aggregates of equally oriented stacks of smectite lamellae for showing how the performance of a microstructural model of smectite clay can be imagined. The model was worked out by Pusch, Muurinen, Lehtikoinen, Bors and Eriksen (1992) and implied, like the earlier mentioned model proposed by Neretnieks and Moreno, different fluxes of Brownian particles in microscopic channels representing an interlamellar space of less than 0.3nm. For the case of steady state transport under a constant macroscopic concentration gradient, the electric field induced by the negatively charged channel walls aligns dipolar particles and reduces their mobility by “electro-viscous” effects. As stated, one usually distinguishes between pore diffusivity (D_p , D_e (“effective” diffusivity, and D_o (“apparent” diffusivity) of which we will make use of the first-mentioned for the sake of simplicity. For being able to use the microstructural F -parameters and for going deeper into structural specification we will use a microstructural model GMM, proposed by Pusch et al (1999) based on void size distributions evaluated from TEM micrographs according to Pusch and Yong (2006), and Bouchelaghem and Pusch (2017). It involves use of Hagen/Poiseuille’s theory of water transmissivity of tubular systems. This requires geometrical modelling of the channels as arrays of hydraulically unconnected parallel capillaries with periodic step-wise changes in channel diameter for calculation of equilibrium ionic distributions within REV’s for three bulk densities as indicated in Table 4. Table 5 shows estimated channel dimensions, and Figure 19 shows schematically the GMM model with the gray bars representing stacks of smectite lamellae, and a specific REV.

Table 4: Microstructural data and conductivities for MX-80 in Ca form saturated and percolated by strongly brackish Ca-dominated water (Pusch and Yong, 2006).

Bulk density/ Bulk dry density [kg/m³]	Gel density (total/dry) [kg/m³]	Measured gel conductivity [m/s]	Calculated bulk conductivity [m/s]	Measured bulk conductivity[m/s]	Porosity
2130/1794	2000/1590	2E-13	3E-14	2E-14	0.13
1850/1349	1650/1030	8E-11	2E-12	2E-12	0.20
1570/904	1150/238	1150	3E-06	2E-09	0.47

**Table 5: Channel dimensions for smectite in Na and Ca form (Pusch, 1999).
Complement to Figure 20.**

Bulk density/Bulk dry density [kg/m ³]	Gel density [kg/m ³]	D1 nm	D2 [nm]	L1 [nm]	L2 [nm]
2130/1794	2000	5	1	10	5
1850/ 1349	1650	10	2	20	10
1570/904	1150	50	3	100	50

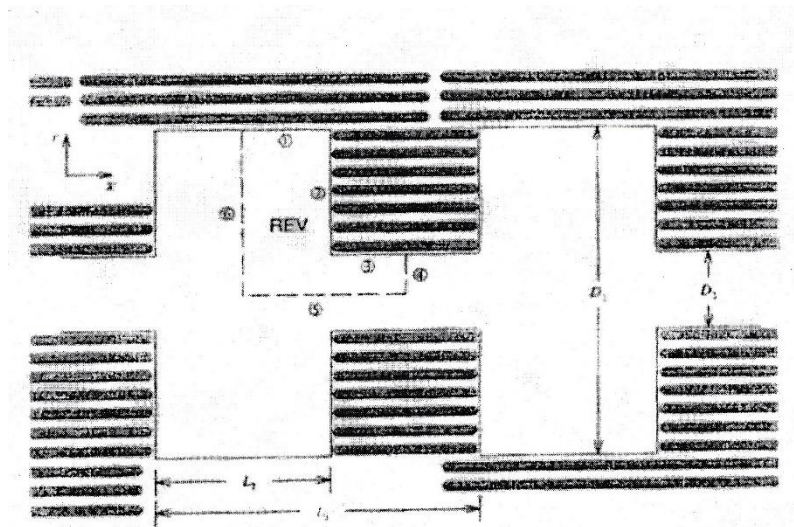


Figure 20: Schematic ultrafine pore geometry of smectite clay (GMM microstructure version).

The anion concentration in a REV for about 1800kg/m³ bulk dry density is of particular practical importance since a density of this order is aimed at for smectite clay seals intended for isolating high-level radioactive waste (Svemar, 2005).

Following the principle proposed by Pusch and Popov (2019) for estimating ion diffusion rate and capacity of dissolved ions including radionuclides one can use the F -parameter F_3 . Relation of this parameter to migration of ions is more complex than the F_2 relation to permeation, since component a interacts by cation adsorption (Kd-effect) and hinders the movement of big molecules due to geometrical obstacles causing tortuosity. Therefore, cations and big molecules in the a -space migrate both by pore and surface diffusion, while in the b -space ion migration is largely caused by pore diffusion. The two microstructural components are related through the coefficients F_2 for 2D and F_3 for 3D conditions. The ratio

F_3/F_2 depends on the average and individual bulk and gel densities as exemplified by Figure 21 and Table 4 for a commercial bentonite (“MX-80”). The concentration of ions migrating by diffusion can be derived by using ordinary diffusion theory (cf. Brandberg et al, 1991).

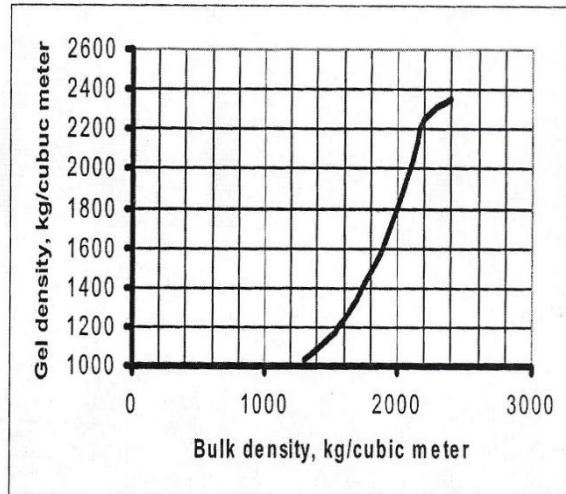


Figure 21: Correlation of the average gel density (r_b) and the average bulk density (r_{av}) for Wyoming bentonite (MX-80).

This procedure for density-related microstructural characterization can be applied to any soil analyzed with respect to the microstructural constitution using micrographs of very thin sections.

F -data together with data for bulk and gel density in kg/cubic meter, as well as calculated and experimental K -values in m/s are shown in Tables 6 and 7 for three representative bulk densities of smectite-rich clay (MX-80), F_3 also being a measure of ion concentration per m^3 . Good agreement is obtained between the model-derived data for artificially prepared Wyoming clay (MX-80) in Na form and experimental results.

Table 6: Microstructural data and conductivities for MX-80 saturated and percolated by strongly brackish Na-dominated water (Pusch and Popov, 2019).

Bulk total density/dry density [kg/m ³]	F_2/F_3	Gel density (total/dry) [kg/m ³]	Experimental gel conductivity [m/s]	Calculated bulk conductivity [m/s]	Experimental bulk conductivity [m/s]
2130/1794	0.17/ 0.07	2000/1590	7E-14	E-14	2E-14
1850/1349	0.24/0.12	1650/1030	2E-12	4E-13	2E-13
1570/904	0.40/0.26	1150/238	2E-10	8E-11	8E-11

Table 7: Microstructural data and conductivities for MX-80 saturated and percolated by strongly brackish Ca-dominated water (Pusch and Popov, 2019).

Bulk total density/dry density [kg/m ³]	F_2/F_3	Gel density (total/dry) [kg/m ³]	Experiment gel conductivity [m/s]	Calculated bulk conductivity [m/s]	Experimental bulk conductivity [m/s]
2130/1794	0.17/0.07	2000/1590	2E-13	3E-14	3E-14
1850/1349	0.24/0.12	1650/1030	8E-11	2E-12	2E-12
1570/904	0.40/0.26	1150/238	7E-5	3E-06	3E-09

The microstructural heterogeneity of artificially prepared MX-80 clay is a significant factor especially for experimental determination of the hydraulic conductivity but also for the ion diffusivity of clay of this kind. In comparison to natural sedimentary clays with the same density and smectite content, the results indicate that higher hydraulic conductivity values are obtained for artificially prepared MX-80 clay since it maintains some of the natural granular form. From the perspective of DDL interactions within the clay matrix, replacement of the original Na⁺ by Ca²⁺, Cd²⁺ and some radionuclides will raise the hydraulic conductivity. If one assumes the same F_2 values and gel densities as for MX-80 in Na form and uses typical gel hydraulic conductivities for MX-80 in Ca form, one obtains the results shown in Table 5 in which the bulk density of MX-80 in virgin form is given in the first column. The results shown in other columns refer to this clay in Ca form. As can be seen, good accord is obtained between calculated and true conductivity data except for the lowest bulk density, which is explained by microstructural heterogeneity caused by coagulation.

Figure 22 shows the calculated equilibrium anion concentration in the REV in Figure 19 for the bulk total density 2130kg/m³ (dry density 1794kg/m³) assuming 0.001, 0.01 and 0.1M monovalent electrolyte and that 10% of the clay particle edges are negatively charged. Anions are confined in the central part of the pore for the 0.001M solution but takes up a larger space for the stronger 0.1M concentration. Cations are located close to the crystallites' surfaces.

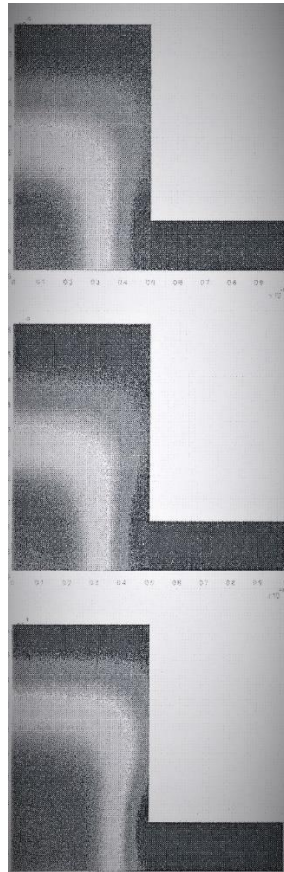


Figure 22: Distribution of ions in the REV with bulk dry density 1794kg/m^3 .

***Upper:* The dark areas “1” and “3” in Figure 20 represent low anion concentration while the bright area “2” represents high anion concentration for 0.001M monovalent electrolyte. *Middle;* The bright area “2” is smaller than for 0.001M solution, and is moved somewhat away from the particle wall for the 0.01M solution. *Lower:* The bright area “2” representing anion concentration for the 0.1M solution has expanded towards the particle wall and reaches the particle wall. Cations are close to the particle walls in all pictures and move along those carrying electrical double layers (After Pusch, Muurinen, Lehtikoinen, Bors and Eriksen, 1992).**

The detailed distribution of electric potentials and cationic concentration of positively charged radionuclides is exemplified by Figure 23, which illustrates predicted diffusion of Sr in soft smectite clay (dry density 400kg/m^3).

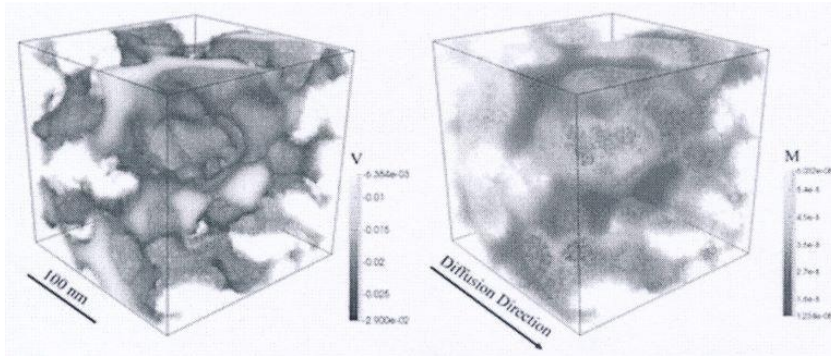


Figure 23: Sr diffusion in smectite with dry density 400kg/m^3 . Left: Electric potential distribution representing a typical aggregated microstructural pattern. Right: Cation concentration distribution with darkest zones indicating dense aggregates of smectite stacks. (After Yang and Wang, 2019).

6.3 Electric potentials and concentration of diffusing radionuclides in smectite clay channels

Referring to Yang and Wang (2019) one can predict the mean cationic concentration in a REV exposed to a constant concentration of cations and anions by utilizing the microstructural parameters F_2 and F_3 . We find the procedure in Table 8.

Table 8: Microstructural data, cation and anion concentrations of for MX-80 clay saturated and percolated by strongly brackish Na-dominated water (Pusch and Popov, 2019). The cationic radionuclide is called NC and the anion considered is called NA.

Bulk total density/dry density [kg/m^3]	Total water content in b -space [kg/m^3]	F_2/F_3	Gel density (total/dry) [kg/m^3]	Mean NC concentration at constant gradient in a -space [kg/m^3]	Mean NA concentration at constant gradient in b -space [kg/m^3]
2130/1794	206	0.17/0.07	2000/1590	F_3 times gel dry density and meq	F_3 times water in b -space
1850/1349	301	0.24/0.12	1650/1030	F_3 times gel dry density and meq	F_3 times water in b -space
1570/904	246	0.40/0.26	1150/238	F_3 times gel dry density and meq	F_3 times water in b -space

6.4 Distribution of channels in smectite clay

The actual distribution of channels representing flow paths has been estimated by examining clay samples of smectite-rich clay (MX-80) that had been percolated for 10 days by 3.5% CaCl₂ solution to which Methylene Blue tracer with 2% concentration had been added (Pusch, 2008). The first 1 mm part from the inflow end was not investigated but the rest of the 15mm thick sample was dried at 105°C and sliced for taking photographs. The water saturated clays had the densities 1950, 1820 and 1720kg/m³ at water saturation corresponding to the dry densities 1510, 1300, and 1140kg/m³, hence resembling those of the reference clays in Tables 3 and 4, and being represented by Figure 24 in which the automatically evaluated accumulated cross section areas of the black spots are given. The percentages varied from about 1.75 to 3.31%, which are somewhat higher than the true values because of the diffusive migration of the tracer from each penetration spot. However, the channel cross section areas and the distribution of the channels are in reasonable agreement with calculated flow data according to the Hagen-Poiseuille channel flow model assuming a pressure difference on the opposite sides of the cubic grid.

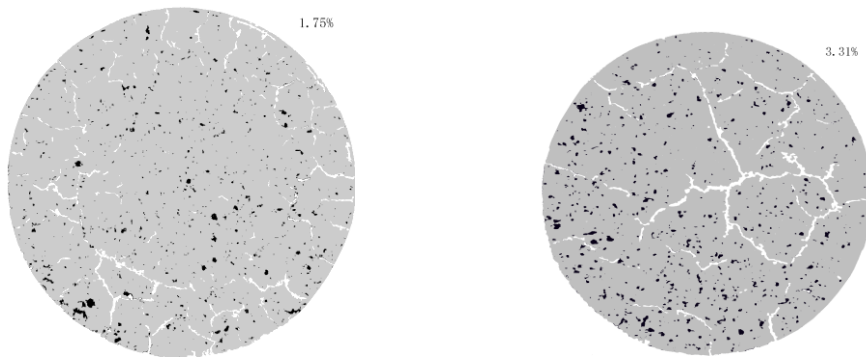


Figure 24: Distribution of permeated channels appearing as black spots in the dried MX-80 samples with 30 mm diameter. *Left:* Sample with density 1950kg/m³ at water saturation (dry density 1508kg/m³). The cross section percentage of black spots of the total cross section was 1.75%. The white objects are desiccation fractures. *Right:* Sample with density 1720kg/m³ at water saturation (dry density 1140kg/m³). The percentage of black spots of the total cross section was 3.31%.

One finds from the digital maps that the distribution of the channels was relatively uniform but that there may be a scale factor that can have had an impact on the ratios. The graphs show that leakage along the clay/cell contact was negligible.

6.5 Interaction of smectite and water under pressure at elevated temperature

The influence of temperature and water pressure on water sorption and particle thickness of montmorillonite clay confined in autoclaves under controlled water pressure conditions has been examined by several investigators. A carefully conducted test comprised a series of experiments on montmorillonite slurry with a fluid content of 800% (dry density 79kg/m^3) that was placed in a cell exposed to temperatures up to 200°C and hydraulic pressures of up to 40MPa (Colten, 1986). The molality of the NaCl solution used for saturation was 1 to 5. This study showed that the interlamellar spacing was negligibly changed in the tests, which is explained by the fact that no effective (“grain”) pressure acted on the clay.

The cations cause polarization of neighbouring water molecules by which their mobility drops and the chemical potential is reduced. Further reduction is due to van der Waals attraction between the hydrates and the adjacent mineral lattice and to hydrogen bonds established between the hydrates and lattice hydroxyls. Interlamellar hydrates are pressed together by the attraction between the lamellae, which increases the chemical potential. It is hence highest for low water contents and higher for interlamellar hydrates than for hydrates on basal surfaces of clay particles. Nakano et al found that the chemical potential of the first hydrate adsorbed on basal surfaces is on the order of $E7\text{ J/kg}$, and about $E2\text{ J/kg}$ for hydrates at around 6nm from the surfaces of the mineral particles.

A similar test series was made on MX-80 clay saturated with distilled water and enclosed in autoclave cells giving high porewater overpressures by heating. The overpressure was $40\text{-}70\text{MPa}$ for temperatures up to 200°C and the swelling pressure of the clay samples, which had a dry density of 480kg/m^3 , was about 70kPa . XRD analysis of sedimented clay specimens demonstrated very small changes in interlamellar spacing, i.e. from 16.7\AA for room temperature to 16.7 to 17.3\AA spacings (001) for samples exposed for 0.5 years to 150 and 200°C , respectively. These data are in fact somewhat higher than for unheated clay and confirm that no permanent contraction or compression took place under the very low effective pressures that prevailed in the course of heat treatment. However, the peak heights were increased by 5 and 50%, respectively, indicating that alignment of stacks of lamellae took place. This process was probably generated by reorientation, compression and shearing of the stacks of lamellae under the actual low effective pressure. It is believed that compression of the stacks was triggered by heat-induced reduction of the strength of the interlamellar hydrate layers.

6.6 Expandability (Swelling pressure)

The swelling pressure exerted on the physical boundaries of smectite clay seals is caused by combination of the true “disjoining” pressure generated by the interlamellar water films, which strive to grow to a certain finite thickness if expansion can take place, and of the osmotic pressure caused by the charge conditions at the outer boundaries of the stacks of lamellae. The swelling pressure-time relationship shown in Figure 25 was obtained from tests on MX-80 montmorillonite-rich clay. The clay sample was prepared by compacting air-dry

clay granules directly in the oedometer, and then allowed to take up water under constant volume conditions. For a smectite-rich clay with a dry density of at least a few hundred kg/m³ the air enclosed in the powder becomes pressurized in the hydrating clay. The air dissolves and diffuses out of the system – a process that occurs even if water uptake is allowed to occur from only one end of the cell. The peak reached after the first day was due to evolution of the microstructure. From a physical standpoint, we can describe this as expansion of the individual dense clay granules and of subsequent movement into more stable positions of aggregates and individual particles, as well as of dispersion of stacks of lamellae exfoliated from dense aggregates, followed by coagulation of these units. In electrolyte-poor water the latter mechanism initially gave low mechanical strength of the coagulate, represented by the first peak, and development of a second peak after a couple of days. In salt water the coagulate is stronger than in electrolyte-poor water.

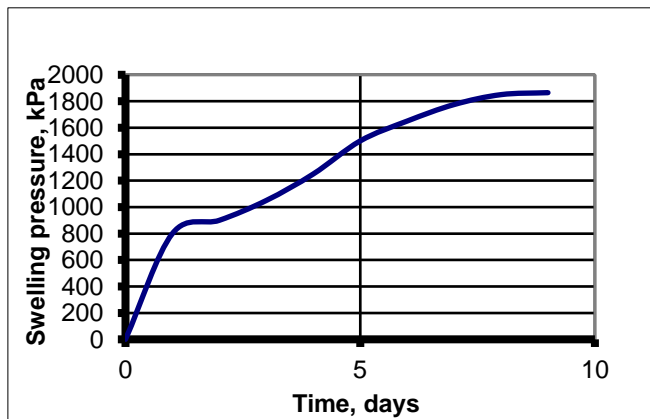


Figure 25: Recorded swelling pressure of maturing clay with about 70% montmorillonite content and 1390kg/m³ dry density (1875kg/m³ at water saturation). The sample was prepared by compression of air-dry MX-80 granules followed by saturation with distilled water.

Typical smectite swelling pressure data are collected in Table 8. The table summarizes values determined by use of oedometer (pressure) cells for characterization of easily available natural smectitic clays after air-drying, crushing and sieving for removal of grains bigger than 2mm. The natural water content is usually 7-15 percent by weight.

Table 8: Swelling pressure (p_s) in MPa of well characterized smectite-rich materials at saturation with distilled water (1800 and 2000kg/m³ total density correspond to the dry densities 1270kg/m³ and 1590kg/m³, respectively).

Density at saturation, kg/m ³	1800	2000
MX-80	0.8-0.9	4-5
IBECO, Na	0.6-1	4-5
IBECO, Ca	0.2	5
Beidellite	1.5	4.2
Saponite	2.5	8.8
Mixed-layer S/I Friedland clay	0.1	0.9

The smectite-rich clays MX-80 and IBECO, which are commercially available in large quantities, have montmorillonite as major smectite constituent (70-90%). Saponite and beidellite behave as montmorillonite for low densities while they develop higher swelling pressures for high densities. For densities higher than about 2000kg/m³ at water saturation the chemical composition of the porewater does not exercise much influence on the swelling pressure because DDL forces are practically non-existent. The low amount of water uptake at very high densities is to all intents and purposes structured pseudo-crystalline interlamellar water. Water uptake beyond hydrate water will be by DDL forces, at which time the density of the samples will be in the medium density range and make the influence of the cation species significant. For lower densities, the chemical composition of the porewater is very important especially for the degree of physical stability.

We will not comment on gas permeability here other than referring to experience (Osipov et al, 2004) and comprehensive gas migration tests indicating that gas penetration and transport in smectite clay is related to the swelling pressure, which has to be exceeded for letting pressurized gas through (Pusch, et al, 1985; Horseman and Harrington, 1997; Wilson et al, 2011).

The swelling pressure is caused by the disjoining forces in the interlamellar space and double-layer repulsion between basal planes. Considering the detailed force distribution in the commonly heterogeneous microstructure, the swelling pressure is estimated to be proportional to the product of the true swelling pressure of the pressure-controlling component a and the volume ratio $(a^3 - b^3)/a^3$ in Figure 12. This ratio is $(1 - F_3)$, which gives the volume fraction of this component. For a bulk density of 2130kg/m³ ρ_a is 2000kg/m³ and the true swelling pressure of this component about 11MPa, according to Yong and Warkentin (1975). The factor $(1 - F_3)$ is 0.93 and the product hence about 10 MPa. For the bulk density 1570kg/m³ ρ_a is 1750kg/m³, and the true swelling pressure about 0.3MPa. The value of $(1 - F_3)$ is 0.75 and the product

about 0.2 MPa. The values are in good agreement with experimental data as illustrated by Table 9.

Table 9: Calculated and experimentally determined swelling pressures (p_s) of MX-80 saturated with distilled water.

Bulk density [kg/m ³]	1- F_3	Density of massive part [kg/m ³]	p_s of massive part [MPa]	Calculate d bulk p_s [MPa]	Experimental bulk p_s [MPa]
2130	0.93	2150	15	14.0	14.0
1850	0.80	1900	1.5	1.2	1.0
1570	0.75	1750	0.5	0.4	0.3

Applying the same generalization as for the hydraulic conductivity, i.e. assuming that the major microstructural features expressed in terms of F_3 , are the same as for saturation with distilled water, one gets, for MX-80 in Ca form, the same theoretical swelling pressure as for MX-80 saturated with distilled water when the bulk density is 1570, 1850 and 2130kg/m³, respectively. These pressure values agree well with experimental results (Pusch and Yong, 2006; Herbert and Kasbohm, 2008). Even for the lowest density at saturation, 1570kg/m³ (dry density 900kg/m³) there is fair agreement but insufficient sensitivity of the simple model for densities representing conditions close to complete expansion of the densest part of the clay matrix (a in Figure 14) indicates heterogeneity. On altering the porewater electrolyte of smectite-rich clay with a density of 2130kg/m³, from low and intermediate saline solution to ocean water salinity, the swelling pressure was unchanged, which is also documented by numerous experiments. For a bulk density of 1850kg/m³ at saturation with distilled water the theoretical value would be about 1.2MPa to be compared with the experimental value 1.0MPa, while for ocean water a typical experimental value is on the order of 0.5MPa. For the lowest bulk density 1570kg/m³ the theoretical and experimentally determined swelling pressure were 0.3-0.5MPa for saturation with distilled water, while recorded swelling pressures for saline water are only a few tens of kPa.

7. Comments and Conclusive Remarks

Smectite clay is used for isolating low-and intermediate-level radioactive waste in on-ground and relatively shallow underground repositories for a few hundred or thousand years Pusch (2008, 2012) and Svemar (2005). Highly radioactive waste that can give off cationic and anionic radionuclides can be more effectively shielded by such clay at medium or large depth if the density is high. The clay seals need to be very dense for minimizing percolation and for providing a high enough swelling pressure that can generate self-healing of local parts with lower density. They have to remain largely impermeable for at least 100,000 years, and be sufficiently ductile to sustain seismic and tectonic impact that would otherwise cause breakage and leakage of the waste canisters. The clay seals are placed around and between waste packages. The objective of the present paper is to illustrate how simple modelling of the maturation of smectite clay seals can be made and how permeation of them takes place by increasing or decreasing the dry density.

We assume in this paper that engineering barriers of smectite clay maintain their chemical and mineralogical constitution for the required operational period of time, as long as the temperature does not exceed about 60°C at which it is assumed to become converted to a high-temperature form, i.e. the one proposed by Hofmann, Endell & Wilm, implying reorganization of lattice hydroxyls. One realizes from the described function of adsorbed cations that exchange from Na to Ca by flooding the repository with saline water has great impact on the physical performance of smectite clay seals with low to moderate density.

An important contribution to the understanding of the role of clay microstructure is the described way of interpreting transmission micrographs for manifesting the heterogeneity of the clay in a form that makes it possible to correlate microstructure and experimental bulk data respecting geotechnical properties of soils.

An equally important finding is that it is possible to define and use microstructural parameters for relating structural features of smectites with their physico-chemical properties and behaviour, a matter that requires deeper study of the chemical stability of smectite minerals used for isolating hazardous waste like highly radioactive waste.

ACKNOWLEDGEMENTS.

The author is greatly indebted to Professor Fatiha Bouchelaghem, Sorbonne University, France, for her excellent work on clay microstructure that was of very significant help in the preparation of the present paper.

References

- [1] Bouchelaghem, F. and Pusch, R. (2017). Clay microstructure: imaging numerical homogenization and correlation with physical data. *Applied Clay Science*, 144, pp.9-18.
- [2] Brandberg, F. and Skagius, K. (1991). Porosity, sorption and diffusivity data compiled for the SKB 91 study. Swedish Nuclear Fuel and Waste Management AB (SKB). Technical Report TR 91-16, SKB, Stockholm.
- [3] Colten, V.A. (1986). Hydration states of smectite in NaCl brines at elevated pressures and temperatures. *Clays and Clay Minerals*, 34, pp.385-389.
- [4] Forslind, E. and Jacobsson, A. (1972). "Clay water systems" in *Water, a Comprehensive Treatise*. F. Franks (ed); Plenum Press, New York.
- [5] Herbert, H., J., Kasbohm, J., Sprenger, H., Fernández, A.M. and Reichelt, C. (2008). Swelling pressures of MX-80 bentonite in solutions of different ionic strength. *Physics and Chemistry of the Earth*, 33, pp.327-342.
- [6] Horseman, S.T. and Harrington, J. F. (1997). Study of gas generation in MX-80 buffer bentonite. British Geological Survey, WE197/7.
- [7] Kehres, A. (1983). Dehydration energy isotherms of clays. Diagrams for surfaces of interlamellar and extralamellar (microvoids) space. PhD Thesis, Université Paul Sabatier, Toulouse, France.
- [8] Neretnieks, I. and Moreno, L. (1993). Fluid flow and solute transport in a network of channels. *Journal of Contaminant Hydrology*, 14, pp.163-192.
- [9] Osipov, V.I., Sokolov, V.N. and Eremeev, V.V. (2004). Clay seals of oil and gas deposits. Balkema Publishers, Lisse/Atingdon/Exton (PA)/Tokyp ISBN 90 5809 90 5809 583.
- [10] Pusch, R., Ranhagen, L. and Nilsson, K. (1985). Gas migration through MX-80 Bentonite. NAGRA Technical Report 85-36.
- [11] Pusch, R. (1987). Identification of Na-smectite hydration by use of "Humid Cell" High Voltage Microscopy. *Applied Clay Science*, 2, pp/343-352.
- [12] Pusch, R. (1993). Evolution of models for conversion of smectite to non-expandable minerals. SKB Technical Report TR-93-33, SKB, Stockholm, Sweden.
- [13] Pusch, R., Muurinen, A., Lehtikoinen, J., Bors, J., Eriksen, T. (1999). Microstructural and chemical parameters of bentonite as determinants of waste isolation efficiency. European Commission Final Report Contr. No. F14W-CT95-0012, European Communities.
- [14] Pusch, R. (1999). Clay colloid formation and release from MX-80 buffer SKB Technical Report TR-99-31. Swedish Nuclear Fuel and Waste Management Co (SKB), Stockholm, Sweden.
- [15] Pusch, R., Moreno, L. and Neretnieks, I. (2001). Microstructural modelling of transport in smectite clay buffer. Proc. Int. Symp. on suction, swelling, permeability and structure of clays. Eds. K Adachi & M Fukue. Balkema, Rotterdam/Brookfield. ISBN: 90 5809 175 9.

- [16] Pusch, R. and Yong, R.N. (2006). *Microstructure of smectite clays and engineering performance*. Taylor & Francis, London.
- [17] Pusch, R. (2008). *Geological storage of radioactive waste*, Springer-Verlag, Berlin, Heidelberg, (ISBN: 978-3-540-77332-0).
- [18] Pusch, R. (2012). The geological basis for developing concepts for disposal of highly radioactive waste (HLW) in crystalline rock – a state of art compilation. *Communicacoes Geologicás*, Vol. 99, No.1, 2012, pp.61-68.
- [19] Pusch, R. (2015). *Bentonite Clay, Environmental Properties and Applications*, CRC Press.
- [20] Pusch, R. and Popov, V. (2019). Micro- and macroscopic ion diffusion controlled by clay microstructure. *Journal of Earth Sciences and Geotechnical Engineering*, Vol.9, No.3, 101-116.
- [21] Sposito, G. (1984). *The surface chemistry of soils*. Oxford University Press, New York, Clarendon, Oxford.
- [22] Svemar, C. (2005). *Cluster repository project (CROP). Final Report of European Commission, Contract FIR1-CT-2000-20023*, Brussels, Belgium.
- [23] Wilson, J., Savage, D., Bond, A., Watson, S., Pusch, R. and Bennett, D. (2011) *Bentonite - A Review of key properties, processes and issues for consideration in the UK context*. Quintessa Ltd., Henley-on-Thames, UK.
- [24] Yong, R.N. and Warkentin, B.P. (1975). *Soil properties and behaviour*. Elsevier Publ. Co, Amsterdam.